



Asian heat stress variations in a changing climate: Implications for disproportionate urban and rural population exposure

Pir Mohammad ^{a,b} , Qihao Weng ^{a,b,c,*} 

^a JC STEM Lab of Earth Observations, Department of Land Surveying and Geo-Informatics, The Hong Kong Polytechnic University, Hung Hom, Hong Kong

^b Research Centre for Artificial Intelligence in Geomatics, The Hong Kong Polytechnic University, Hung Hom, Hong Kong

^c Research Institute of Land and Space, The Hong Kong Polytechnic University, Hung Hom, Hong Kong

ARTICLE INFO

Keywords:

Urban-rural
Climate change
Disparities
Heat stress
Population exposure
SSPs

ABSTRACT

The changing climate has intensified the occurrence of extreme heat events, posing a huge challenge for sustainable development and necessitating the implementation of suitable measures to address these issues. Large scale disparities in heat stress over the selected geographic and climatic regions of Asia and the different urban-rural population exposure to heat stress under different climate change scenarios is not well understood. Here, using long-term modelled data in both historical (1990–2014) and four future (2026–2100) SSP (shared socio-economic pathway) scenarios, we evaluated the heat stress variability across time and space in different geographic setting of Asia and mapped the heat stress population exposure for urban and rural region separately. We found a pervasive disparity in heat stress magnitude and trend over different regions of Asia and a noteworthy escalation of heat stress in future SSPs scenarios, with a more profound effect under the SSP5-8.5 and SSP3-7.0. Moreover, a substantial increase in population exposure to heat stress is evident in both urban and rural contexts, with large inequalities in urban and rural population exposure in Eastern China. Our results provide a quantitative estimate of the heat stress and its urban-rural population exposure, which will provide valuable insights for authorities and policymakers, highlighting the importance of the need for sustained emergency investment on a priority basis for most vulnerable populations in future heat wave occurrence.

1. Introduction

Climate change is creating serious repercussions around the world, posing unforeseen challenges to human health and the environment (Campbell-Lendrum et al., 2023; Garschagen, 2016). Global warming is a key issue in climate change and has significantly accelerated many climate-related disasters and extreme weather events. One of the deadliest and costliest disasters is extreme heat wave events, which caused more than 0.15 million casualties globally and caused an economic loss of around 61 billion USD between 1998 and 2017 (Wallemacq & House, 2018). In recent decades, the focus of climate change research has increasingly turned to heatwaves, propelled by the rapid pace of global warming. It has become more intense, frequent, and long-lasting in the twenty-first century (Meehl & Tebaldi, 2004; Nanditha et al., 2020) and is projected to be more deadly in the future (Alizadeh et al., 2022). Indeed, the impact of heat stress on human resources is much higher than other extreme disasters (Dovie & Pabi, 2023). It causes an inevitable negative impact on water scarcity,

heat-related mortality, agriculture, and other socioeconomic aspects (Rohini et al., 2019). Additionally, population exposure to future heat-wave conditions will be increasing by manifold (Lohrey et al., 2021; Ullah, 2022a), compared to the 30% present-day global population exposure to climatic conditions exceeding the deadly threshold for at least 20 days a year (Mora et al., 2017).

Previous studies used maximum and minimum temperatures to characterize daytime and nighttime heat wave (HW) phenomena (Qin, 2022; Ullah, 2022b). Downscaled satellite-derived land surface temperatures were also used to assess health risks associated with heat waves (Jiang et al., 2015). However, temperature alone cannot provide a clear representation of the impact of heatwaves on human health. Higher humidity can exacerbate heat stress for individuals with lower body temperature conditions, which creates an environment where the human body cannot cool, leading to potentially harmful health risks. Thus, the role of humidity is undeniable in heat stress assessment (Cvijanovic et al., 2023; Mora et al., 2017), as it directly influences the level of discomfort and health risks associated with higher temperatures.

* Corresponding author. Research Centre for Artificial Intelligence in Geomatics, The Hong Kong Polytechnic University, Hung Hom, Hong Kong.
E-mail address: qihao.weng@polyu.edu.hk (Q. Weng).

By utilizing the wet bulb globe temperature (WBGT) as a heatwave indicator, a notable rise in population exposure to future heat waves was observed in South Asia (Ullah, 2022a). The increasing demand for land, water, physical infrastructure, and industrialization in urban areas exacerbate heat stress and other climate disaster (Kibwami & Tutesigensi, 2016). In a warming world, heat waves have already occurred in approximately 45% of the global land area (excluding Antarctica), considering daily maximum temperature as HW indices and the average growth rate of global HWs are projected to increase by 2–3 times in SSP2-4.5 and 3–5 times in SSP5-8.5 future scenarios (Yin et al., 2022).

The Asian region, hosting approximately two-thirds of the world's population, is characterized by diverse climatic conditions varying from dry in western Asia to humid and temperate climates in Eastern and Southeastern Asia. The combination of hot summer temperature and humidity, rapid urbanization rate, varied topography, climate variability, and limited coping capacity result in a higher risk of heat stress in this region (Khan et al., 2019; Liu et al., 2021). Certain heat waves in Asia have made a remarkable mark in history due to their significant impact on heat-related mortality. For example, the 2015 Indian heat wave claimed more than 2000 lives when temperatures soared above 45 °C (Hussain et al., 2016). Japan witnessed an intense heat wave event in 2019 that killed more than 100 people and hospitalized tens of thousands (Wang et al., 2019). Recent studies indicate that Japan has experienced over 1000 heat stroke deaths in recent years, which pertains to exposure to excessive heat (Fujibe, 2023). Previous studies emphasized the significance of atmospheric background conditions in influencing three distinct types of heat waves (daytime, nighttime, and daytime-nighttime compound HWs) across China (Xie & Zhou, 2023). The Persian Gulf region of Southwest Asia will surpass the upper limit of wet bulb temperature of human tolerance by the end of this century (Pal & Eltahir, 2016).

The heat stress variability over different regions of Asia has been studied separately either by considering temperature- or temperature-humidity-based indices. However, there is a need for a comparative study that encompasses the entire Asian region, considering its diverse climatic conditions and varying urban-rural population growth trajectories of different countries based on the level of economic development. To effectively characterize heat stress conditions, selecting proper heat stress indices is crucial. Accordingly, this study incorporated a recently developed lethal heat stress index, as it involves a relative humidity correction to wet bulb temperature to better reflect the heat stress situation (Wouters et al., 2022) to assess the variability of daytime and nighttime heat stress over selected geographical and climatic regions of Asia (excluding Russia and Mongolia). Previous studies ignore the SSP3 projection scenario in mapping heat stress population exposure (Ullah, 2022b; Yin et al., 2022), which shows the most substantial population change. Therefore, this study considers all four SSP scenarios to comprehensively assess future population exposure to heat stress. Additionally, population exposure has been estimated separately for urban and rural areas, a new contribution in this research compared to the total population used previously. In addition, this study considers temporal dimensions by dividing the future impact into three distinct time frames: short-term, medium-term, and long-term, as the population changes and heat stress trends vary over time. This approach would allow for a more nuanced analysis of the heat stress variability and enable a better understanding of the impact of heat stress in each future time frame. Examining the future heatwave conditions in various SSP scenarios and population exposure in different selected urban and rural areas of Asia will be extremely helpful for planners and policy makers in formulating heat-related mitigation strategies.

2. Material and methods

2.1. Data

2.1.1. CMIP6 daily modelled data

In this research, we utilized daily near-surface air temperature and relative humidity data from the 26 different global climatic models (GCMs) of the Coupled Model Intercomparison Project Phase 6 (CMIP6) data archive (<https://esgf-node.llnl.gov/search/cmip6/>) (Eyring et al., 2016). The data retrieval process followed the data request guideline (Jukes et al., 2020), specially designed to prepare the IPCC Sixth Assessment Report (AR6). The datasets included both the historical (1990–2014) and the future (2026–2100) periods under four different shared socioeconomic pathways (SSPs) scenarios (SSP1-2.6, SSP2-4.5, SSP3-7.0, and SSP5-8.5), representing the socioeconomic development pathways under the simulated influence of radiative forcing, aerosol emission, and emission from different greenhouse gases (Vuuren et al., 2011), under different levels of representative concentration pathways (RCPs) of RCP2.6, RCP4.5, RCP7.0, and RCP8.5, respectively (Gidden et al., 2019; O'Neill et al., 2016). The selected SSPs scenario identified previously with the higher change in temperature and population exposure to heat stress (Li et al., 2018; Ullah, 2022a). Since the reference (i.e., the historical) period was from 1990 to 2014 of 25 years duration, so in consistent with this period, we divided our 75 years of future data (2026–2100) into three different periods of equal intervals of 25 years from 2026–2050, 2051–2075, and 2076–2100 representing the short-, medium-, and long-term impacts.

The selected model provides data for daily maximum and minimum values of both near-surface air temperature and relative humidity. For diurnal heat stress analysis, we chose four variables: near-surface maximum air temperature (T_{max}), minimum air temperature (T_{min}), maximum relative humidity (RH_{max}), and minimum relative humidity (RH_{min}) under one historical and four future scenarios. Each historical scenario in the models includes four variables, and similar four variables in each Shared Socioeconomic Pathway (SSP) scenario. This results in a total of sixteen variables across the four SSP scenarios. Consequently, each model encompasses twenty variables in total. We selected only those models that provided at least eight variables for our analysis. This led to the final selection of 26 different GCM models developed by different countries at different spatial resolutions (Table 1). All the GCMs models were selected based on the first simulation variant (r1i1p1f1) for each scenario. The details of the number of available models and the presence of selected temperature and relative humidity variables in each model of the five different scenarios are shown in Fig. 1. Due to variations in spatial resolution among CMIP6 model data, it is essential to resample the data to a consistent resolution of $0.5^\circ \times 0.5^\circ$ grid using the bilinear spatial interpolation technique (Zhai et al., 2020). Finally, the ensemble mean of all the selected models for each variable of each scenario was considered because the ensemble mean data was superior in representing the climatic variability than the individual model (Simpson et al., 2021; Ullah, 2022b).

2.1.2. Population data

Mapping the population exposure to heat stress in future projected scenarios is essential for preparedness and determining necessary mitigation strategies. The future projected socioeconomic data is provided by various organizations like the World Bank, United Nations, etc. This study considered annual historical population data provided by the Inter-Sectoral Impact Model Intercomparison Projects of protocol 2b (ISIMIP2b, available at <https://www.isimip.org>) covering the time period of 1861–2005 at a horizontal spatial resolution of 5 arc-minutes ($\sim 0.083^\circ$) (Goldewijk, 2017). The future projected population data was obtained from the SEDAC (NASA Socioeconomic Data and Application Center, available at <https://sedac.ciesin.columbia.edu>) website covering a period of 2010–2100 having 10 years interval with 7.5 arc-minutes ($\sim 0.125^\circ$) spatial resolution (Jones & O'Neill, 2016; 2020).

Table 1
List of the selected CMIP6 models and their detailed information.

S, No.	Model	Developing institute and country	Spatial resolution (in degrees)	Reference
1	ACCESS-CM2	CSIRO-ARCCSS, Australia	1.9 × 1.3	Bi et al. (2013)
2	ACCESS-ESM1-5	CSIRO, Australia	1.9 × 1.3	Law et al. (2017)
3	AWI-CM-1-1-MR	AWI, Germany	1 × 1	Semmler et al. (2020)
4	BCC-CSM2-MR	BCC, China	1 × 1	Wu et al. (2019)
5	CanESM5	CCCma, Canada	2.8 × 2.8	Swart et al. (2019)
6	CMCC-ESM2	CMCC, Italy	1 × 1	Lovato et al. (2022)
7	EC-Earth3	EC-Earth-Consortium, Europe	0.7 × 0.7	Massonnet et al. (2020)
8	EC-Earth3-AerChem	EC-Earth-Consortium, Europe	0.7 × 0.7	Van Noije et al. (2021)
9	EC-Earth3-CC	EC-Earth-Consortium, Europe	0.7 × 0.7	EC-Earth (2021)
10	EC-Earth3-Veg	EC-Earth-Consortium, Europe	0.7 × 0.7	Wyser et al. (2020)
11	EC-Earth3-Veg-LR	EC-Earth-Consortium, Europe	0.7 × 0.7	Ec-Earth, 2020
12	FGOALS-g3	CAS, China	2 × 2.3	Li et al. (2020)
13	GFDL-CM4	NOAA-GFDL, USA	2.5 × 2	Held et al. (2019)
14	GFDL-ESM4	NOAA-GFDL, USA	1.3 × 1	Dunne et al. (2020)
15	INM-CM4-8	INM, Russia	2 × 1.5	Volodin et al. (2018)
16	INM-CM5-0	INM, Russia	2 × 1.5	Volodin et al. (2017)
17	IPSL-CM6A-LR	IPSL, France	2.5 × 1.3	Boucher et al. (2020)
18	KACE1-0-G	NIMS-KMA, Republic of Korea	2.5 × 2.5	Byun et al. (2019)
19	MIROC6	MIROC, Japan	1.4 × 1.4	Tatebe et al. (2019)
20	MPI-ESM1-2-HR	DKRZ, Germany	1.9 × 1.9	Gutjahr et al. (2019)
21	MPI-ESM1-2-LR	MPI-M, Germany	1.9 × 1.9	Mauritsen et al. (2019)
22	MRI-ESM2-0	MRI, Japan	1.1 × 1.1	Yukimoto et al. (2019)
23	NESM3	UIST, China	1.9 × 1.9	Cao et al. (2018)
24	NorESM2-LM	NCC, Norway	2.5 × 1.9	Seland et al. (2020)
25	NorESM2-MM	NCC, Norway	1 × 1	Seland et al. (2020)
26	TaiESM1	AS-RCEC, Taiwan	1 × 1	Lee and Liang (2020)

*Commonwealth Scientific and Industrial Research Organization- Australian Research Council Centre of Excellence for Climate System Science (CSIRO-ARCCSS), Commonwealth Scientific and Industrial Research Organization (ARCCSS), Alfred Wegener Institute (AWI), Beijing Climate Center (BCC), Canadian Centre for Climate Modelling and Analysis (CCCma), The Euro-Mediterranean Center on Climate Change (CMCC), Chinese Academy of Sciences (CAS), National Oceanic and Atmospheric Administration- Geophysical Fluid Dynamics Laboratory (NOAA-GFDL), Institute for Numerical Mathematics (INM), Institute Pierre Simon Laplace (IPSL), National Institute of Meteorological Sciences/Korea Meteorological Administration (NIMS- KMA), Model for Interdisciplinary Research on Climate (MIROC), Deutsches Klimarechenzentrum (DKRZ), Max Planck Institute for Meteorology (MPI-M), Meteorological Research Institute (MRI), Nanjing University of Information Science and Technology (NUIST), NorESM Climate modeling Consortium (NCC), Academia Sinica - Research Center for Environmental Changes (AS-RCEC).

The projected population data was generated according to new SSPs scenarios considering the population growth trend, educational development, urbanization rate, and gross domestic product (Jones & O'Neill, 2016). In addition to the total population, the datasets used in this study also provide information on urban and rural populations at the pixel level, which was used to map the urban and rural populations' exposure to heat stress. The urban and rural population is defined based on the Global Urban-Rural Mapping Project (GRUMP). It distinguishes urban and rural areas based on a combination of population counts (persons), settlement points, and the presence of nighttime light. Areas are defined as urban where contiguous lighted cells from the nighttime lights or approximated urban extents based on buffered settlement points for which the total population is greater than 5000 persons. The gravity-based algorithm is used to reallocate the total population in each administrative unit into rural and urban areas while reflecting the UN national rural-urban percentage estimates as closely as possible. Previous studies on heat exposure mapping predominantly focused on considering total population (Alizadeh et al., 2022; Fotso-Nguemo et al., 2023; Mora et al., 2017; Qin, 2022; Tuholske et al., 2021; Ullah 2022a, b). Thus, separating urban and rural population exposure in this study is a significant novelty.

2.2. Methods

2.2.1. Biased correction and statistical validation of CMIP6 data

Bias correction is the process of adjusting model output to account for biases or discrepancies between the model output and observations. The present study considered additive scaling factor techniques, which is one of the most commonly used statistical methods of bias correction between the observed and modelled data in a reference historical period and ensure an incessant transition into the future (Alizadeh et al., 2022; Freychet et al., 2022; Liu et al., 2020; Qin, 2022; Sun et al., 2022; Ullah 2022b). A mean correction additive factor was calculated for each variable based on the difference between the historical CMIP6 and observed ERA5 data. This additive mean correction factor was consequently applied to both historical and projected datasets. The reanalysis data from the European Centre for Medium-Range Weather Forecasts of the fifth global atmospheric reanalysis (ECMWF-ERA5) at a spatial resolution of 0.25° × 0.25° (Hersbach et al., 2020) has been used as the observed data to find the correction factor for the CMIP6 modelled data. ERA5 data spanning the period from 1990 to 2014 was chosen and resample to 0.5° × 0.5° using the bilinear interpolation technique to ensure consistency with the reference historical data. The performance of each model in simulating selected parameters was evaluated against the reanalysis data using the relative root-mean-squared (Table 2). It has been seen that air temperature gave better performance than relative humidity. The maximum relative humidity showed lower performance, which accounted for the overestimation due to model supersaturation, surface air moisture fields, and false isobaric level field representation (Ruosteenoja et al., 2017). Furthermore, the ensemble mean of all the models is always better than the individual models because the averaging from multiple models can reduce the uncertainties and internal variabilities (Qin, 2022; Saeed et al., 2021; Xu et al., 2021; Yin et al., 2022).

2.2.2. Lethal heat stress index estimation

The potential impact of heat stress on human health is a function of both temperature and relative humidity. Higher temperatures could not significantly affect human comfort working outdoors. The combined effect of higher temperature and relative humidity burden human thermal comfort, psychomedical health issues, and labour productivity due to the reduced capacity of the human body to regulate its own body temperature via perspiration as air humidity increases (Buzan & Huber, 2020; Mora et al., 2017; Pal & Eltahir, 2016). Previously, many studies considered wet bulb temperature (T_w) in identifying heat stress days (Im et al., 2017; Saeed et al., 2021; Ullah 2022a). T_w resembles the

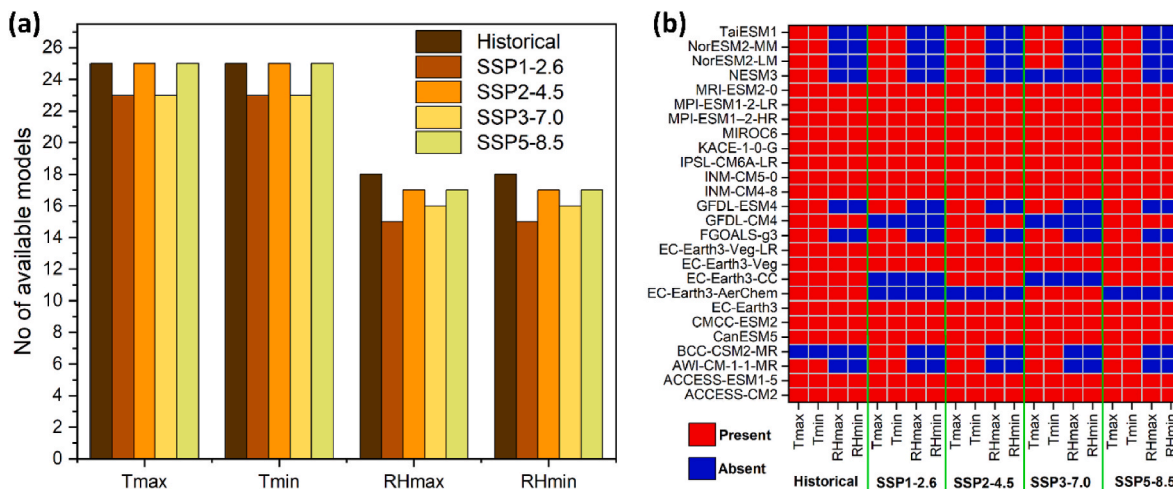


Fig. 1. Detail of the available historical and four future scenarios of 26 selected CMIP6 models (a) no of models available in each scenario, (b) available temperature and relative humidity (both maximum and minimum) data in each model.

Table 2

Performance evaluation of selected variable of all the 26 CMIP6 models and their ensemble mean with respect to the ERA5 observation during the historical period (1990–2014). The relative RMSE of each model is derived as $RMSE' = (RMSE - RMSE_{median}) / RMSE_{median}$, where $RMSE$ is the root-mean-squared error of each model and $RMSE_{median}$ is the median of all 26 models.

Model	RMSE'			
	T_{max}	T_{min}	RH_{max}	RH_{min}
ACCESS-CM2	-0.36	-0.45	-0.03	-0.26
ACCESS-ESM1-5	-0.12	-0.19	0.36	0.11
AWI-CM-1-1-MR	-0.32	-0.33	-0.21	-0.36
BCC-CSM2-MR	0.11	-0.09	0.08	-0.17
CanESM5	-0.39	-0.28	-0.12	-0.41
CMCC-ESM2	0.23	0.31	0.56	0.23
EC-Earth3	-0.46	-0.66	-0.22	-0.49
EC-Earth3-AerChem	-0.38	-0.59	-0.31	-0.52
EC-Earth3-CC	-0.39	-0.52	-0.12	-0.44
EC-Earth3-Veg	-0.51	-0.62	-0.42	-0.51
EC-Earth3-Veg-LR	-0.49	-0.46	-0.11	-0.42
FGOALS-g3	0.23	0.36	0.62	0.46
GFDL-CM4	-0.62	-0.56	-0.23	-0.41
GFDL-ESM4	-0.55	-0.51	-0.41	-0.53
INM-CM4-8	-0.46	-0.49	-0.09	-0.36
INM-CM5-0	-0.49	-0.48	0.66	-0.23
IPSL-CM6A-LR	0.32	0.12	0.29	0.08
KACE-1-0-G	0.22	0.01	0.38	0.10
MIROC6	0.39	0.46	0.52	0.22
MPI-ESM1-2-HR	-0.23	-0.31	0.09	-0.22
MPI-ESM1-2-LR	-0.32	-0.44	-0.01	-0.38
MRI-ESM2-0	0.26	0.06	0.24	0.19
NESM3	0.46	0.52	0.52	0.41
NorESM2-LM	-0.21	-0.36	-0.06	-0.41
NorESM2-MM	-0.33	-0.42	-0.21	-0.44
TaiESM1	-0.29	-0.22	1.32	-0.19
Ensemble	-0.76	-0.71	-0.45	-0.64

thermoregulation process of a human body. It reflects the temperature of a body by evaporative cooling at constant pressure, until it reaches saturation (Meehl & Tebaldi, 2004). Indeed, the evaporative cooling (perspiration) in low level enthalpy conditions, where body discharges more metabolic heat, prevents potentially fatal hyperthermia, even when exposed to air temperature higher than the body's core temperature of ~37 °C (Sherwood & Huber, 2010).

In view of this Wouters et al. (2022), developed an index called Lethal Heat Stress (T_s) index based on wet bulb temperature (T_w) and relative humidity (rh) as shown in Eq. (1).

$$T_s = T_w + 4.5 \left(1 - \left[\frac{rh}{100} \right]^2 \right) \tag{1}$$

The wet bulb temperature (T_w) can be calculated using air temperature and relative humidity following the empirical equation from (Stull, 2011) as shown in Eq. (2).

$$T_w = T^* \arctan \left[0.151977^* \left((rh + 8.313659)^{\frac{1}{2}} \right) \right] + \arctan(T + rh) - \arctan[rh - 1.676331] + 0.00391838^* rh^{\frac{3}{2}} \arctan(0.023101^* rh) - 4.686035 \tag{2}$$

where, T is the air temperature (°C), and rh is the relative humidity (%). The arctangent function uses argument values as if they are in radians. The equation is valid for a pressure of 101.325 kPa, and the saturation corresponds to liquid water over all temperatures. He also calculated errors in his estimation and found that the fraction of variance (r^2) estimated by the regression was 99.95%.

The lethal heat stress index, developed by Wouters et al. (2022), performs well in varying humidity conditions due to adding a second term to the wet bulb temperature, which removes the impact of air dryness. A correction factor of humidity is applied [i.e. $4.5 \left(1 - \left[\frac{rh}{100} \right]^2 \right)$] to wet bulb temperature to better reflect the heat stress conditions under low relative humidity conditions. This term collapses to zero when RH reaches 100%, under which dissipation of metabolic heat through sweating becomes ineffective. Using this definition of T_s allows us to assess human heat stress under different meteorological conditions, as the isopleths of constant T_s resemble combinations of daily mean air temperature and relative humidity. In low humidity conditions, drier soils tend to increase the air temperature because of sensitive heating. In such low humidity conditions, adding the second term to wet bulb temperature removes the impact of air dryness as T_s better reflects the humidity distribution despite the lower temperature. Recent studies have emphasized the significance of T_s in accurately identifying days with dangerous outdoor heat wave conditions. (Mohammad & Weng, 2024).

The second term [i.e. $4.5 \left(1 - \left[\frac{rh}{100} \right]^2 \right)$] of Eq. (1) is added to T_w to better reflect the heat stress condition in low-level relative humidity

conditions (Mora et al., 2017). T_s performs better in extremely hot regions like Arabian Peninsula as it shows better heat stress condition of low T_s despite high temperature due to offsetting impact of air dryness (Wouters et al., 2022). Additionally, the index proves to be valuable in other regions, such as India and China. Here, it better reflects the distribution of specific humidity compared to other temperature-based indices, even though the overall temperatures may be comparatively lower. This is particularly important in densely populated areas where high humidity levels can exacerbate the effects of heat. By effectively capturing the nuances of temperature and humidity interactions, this index serves as a vital tool for assessing heat-related health risks and implementing timely protective measures in vulnerable populations.

Previously, studies used absolute or percentile-based thresholds to define warm spells of heat stress days (Alizadeh et al., 2022; Fotso-Nguemo et al., 2023; Ullah 2022a). However, combining both criteria is superior in identifying the warm spell compared to a single criteria method. Relying on a single criterion may lead to misclassification. For example, a temperature threshold alone might classify a short period of elevated temperatures as a warm spell, while failing to account for its duration or context. By integrating multiple criteria, such as temperature thresholds and duration, we can gain a more holistic view of warm spells. The study considered the combining approach and estimated the lethal hot spells following the criteria set by Wouters et al. (2022), where hot spells were defined as days during which the average T_s should not be lower than 19 °C and exceed its 95th percentile summer mean. Based on his findings, thresholds of $T_s = 19$ °C and $T_s = 27$ °C agree with the empirically derived lethal and deadly thresholds of heat stress. It shows that air temperature and air humidity most accurately distinguished between past lethal and nonlethal heat episodes, whereas other meteorological parameters, including radiation and wind, only lead to minimal increases of accuracy. Therefore, we only considered air temperature and humidity in the analysis. Additionally, the minimum mortality temperature is attributed to the regional difference in climatology. For instance, populations in hotter climates may have a higher tolerance to elevated temperatures due to acclimatization, while those in cooler regions may be more susceptible to heat stress even at lower temperatures. In this study, summer is defined per location as the three consecutive months with the highest average T_s . Therefore, the definition of a hot spell in this study accounts for these regional variations, it may risk misrepresenting the actual impacts of heat events on different populations.

2.2.3. Temporal trend of heat stress index

Non-parametric modified Mann-Kendall test developed by Mann (Mann, 1945; Hamed & Ramachandra Rao, 1998) and Kendall (Kendall, 1975) had been used to detect the presence of temporal trends in the time series datasets. One of the major advantages of using this test is that it can detect both linear and nonlinear trends effectively and has been found to be effective in detecting trends in the climatological long-term dataset (Li & Wang, 2022; Malik et al., 2020; Mohammad & Goswami, 2021). The magnitude of the trend was estimated by the non-parametric Sen's slope estimator method (Sen, 1968).

2.2.4. Population exposure to heat stress

The population exposure to heat stress was quantified by multiplying the number of hot spell events by the population. The population exposure for historical and future scenarios has been calculated in a 25-year mean period (Batibeniz et al., 2020; Liu et al., 2020). The 25-year mean population exposure (E_p) was estimated at each grid cell using Eq. (3).

$$E_p = \frac{\sum_{i=1}^{25} HW_i \times P}{25} \quad (3)$$

where i is the i th year of study, HW_i is the annual hot spell days, and P is the population (urban or rural) at that period. The population of that

period is obtained using the mean of the decadal population data used in this study. The urban and rural population exposure to heat stress is calculated separately using the different urban-rural population layers.

3. Results

3.1. Changes in historical lethal heat stress

The daytime T_s exhibits a warmer pattern along the coastal region of the Arabian Peninsula, Indo-Pak border, coastal Indian region, Indo-Gangetic Plain, Eastern China, and Indonesia (Fig. 2a). Contrary to daytime T_s , the distribution of mean T_s at nighttime is more homogeneous over the coastal regions of Arabian Peninsula (Fig. 2b). Considering the mean T_s variation across all the selected cities (with more than 300k population (He et al., 2021)), the cities located along the Indo-Gangetic Plain, the west coast of India, and Eastern China show the highest mean daytime T_s compared to other cities. However, at nighttime, the number of cities showing higher mean T_s decreases, especially in the Eastern China region. The trend analysis result suggests a more significant warming trend over arid climatic areas of the Arabian Peninsula as compared to tropical climate conditions of India and Eastern China in both daytime and nighttime (Fig. 2c and d).

To enhance our comprehension of the distribution of T_s , we divided the study area into four distinct geographic regions with different climatic conditions (Table 3), denoted as R1 to R4 (Fig. 2a). The result shows a higher mean T_s over the R4 region in the daytime and the R2 region in the nighttime (Fig. 2e). It is important to note that despite the comparatively lower mean T_s in region R1, it exhibits a higher Sen's slope trend in both daytime and nighttime (Fig. 2h).

The distribution of summer monthly T_s across the four selected geographical regions shows distinct behaviors, with different peak months observed during daytime and nighttime (Fig. 3). The peak mean T_s was observed in the month of July–August in the daytime and in August during nighttime over region R1. In region R2, the peak mean T_s occurred in June during the daytime and in July during the nighttime. For region R3, the peak was in July for both daytime and nighttime. Lastly, in region R4, the peak mean T_s occurred in April during the daytime and in May during the nighttime. When comparing all four regions together during the daytime, the maximum mean T_s was observed in April and May in region R4, whereas the minimum was in April of region R1. During the nighttime, there is a shift in the mean T_s monthly behaviour, with maximum mean T_s in July of region R2 and minimum in April of region R3.

3.2. Projected changes in lethal heat stress

The selected Asian region shows a significantly higher mean T_s in both daytime and nighttime, noticeable along the coastal region of the Arabian Peninsula, Indo-Gangetic Plain, and Eastern China under all four selected SSP scenarios (Fig. 4a). The results of the four scenarios show a progressive expansion of the higher T_s , which will be more widespread in mitigation challenge-dominated scenarios (SSP5-8.5) and high challenge scenarios (SSP3-7.0) with high GHG forcing. There has been a significant warming of T_s , as revealed by Sen's slope trend over region R1 in the SSP3-7.0 and SSP5-8.5 scenarios in both daytime and nighttime compared to the other three regions (Supplemental Fig. S1). The mean T_s variation in cities signifies a noticeable transformation of lower T_s (green, 34–38 °C) to higher T_s class (black, >38 °C) from the SSP1-2.6 to SSP5-8.5 scenarios in both daytime and nighttime. This transformation is particularly evident in Eastern China and North-western India (Fig. 4a). This signifies a potential shift towards higher extremes, indicating increased heat stress and adverse climatic conditions.

During the historical period, the cities situated in Bangladesh, Cambodia, India, Indonesia, Myanmar, Pakistan, Thailand, UAE, and Vietnam show higher mean T_s classes in the daytime (>24 °C) and

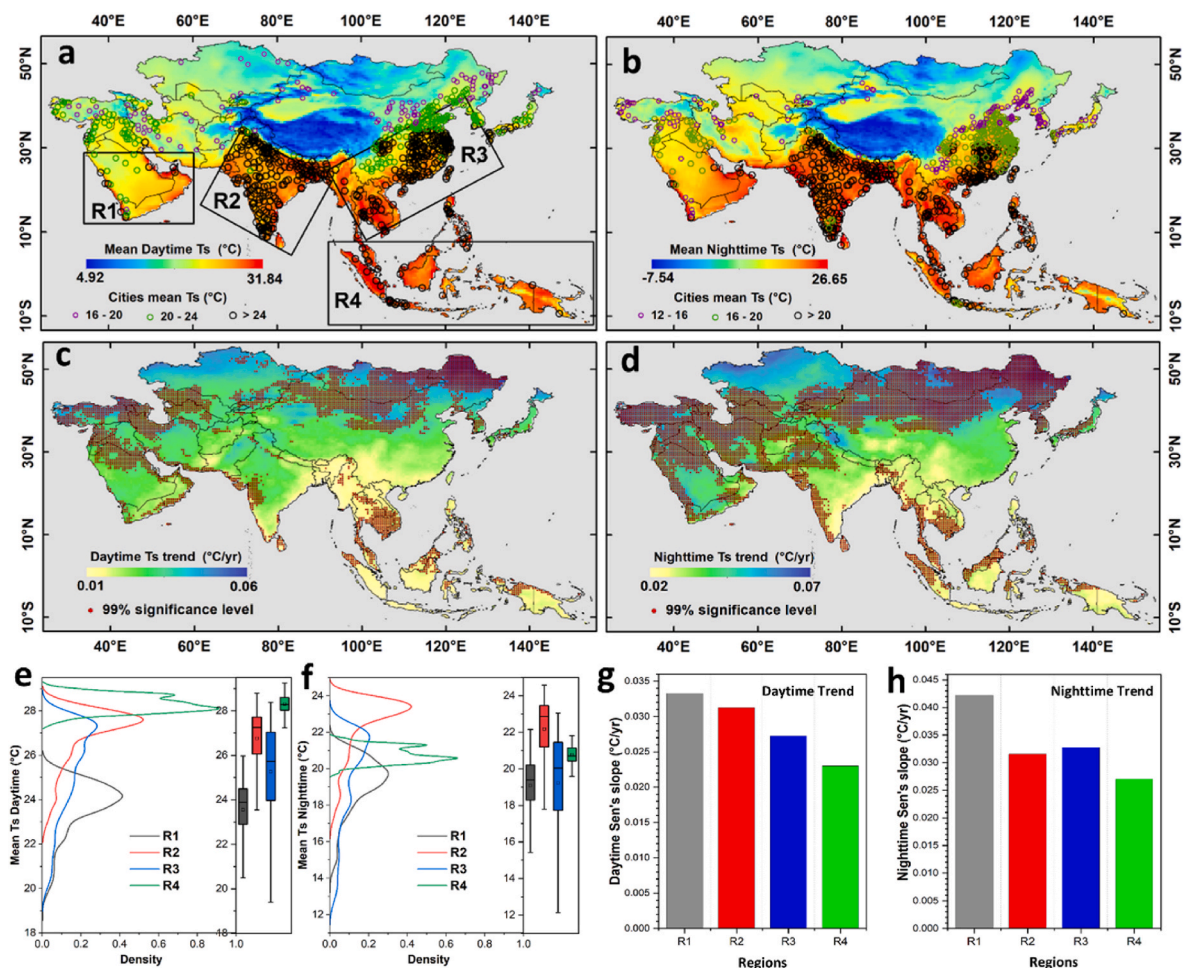


Fig. 2. Historical lethal heat stress (Ts) variation over selected Asian regions. (a) Spatial distribution of the mean Ts average over 1990–2014 during the daytime along with the mean Ts of different cities with populations greater than 300k population (marked in circles), (b) same as a for nighttime, (c) Sen's slope trend from 1990 to 2014 with a 99% significance level marked as red dots during daytime, (d) same as c for nighttime, (e) variation in the mean annual Ts over the four selected geographic regions (R1, R2, R3, and R4; as marked in (a)) in daytime, (f) same as f for nighttime, (g) mean Sen's slope trend value over the four geographic regions in daytime, (h) same as g for nighttime. (For interpretation of the references to colour in this figure legend, the reader is referred to the Web version of this article.)

Table 3
Characteristics feature of the four selected geographical region.

Region	Characteristics
R1	It is characterized of the arid climatic condition of the Arabian Peninsula. The water surface has influenced this region from three sides, which could act as a source of moisture to the area. It is surrounded by Arabian sea in the eastern side, the Red Sea on the southwestern side, and the Persian Gulf on the northwestern side.
R2	This region covers the Indian peninsula and is surrounded by the Arabian sea on the western side and the Bay of Bengal on the eastern side. In the north, it is bounded by the Indian Himalaya, which acts as a barrier to the moisture content coming from the oceans. It also includes the Indo-Gangetic Plain region, the most densely populated region of the world.
R3	It covers mainly the highly densely eastern regions of China, Myanmar, and Thailand. This region has only sea influence from the eastern side. East China, South China, and the Philippine Sea majorly influence this region.
R4	This region includes Southeastern Asian countries like Indonesia and Malaysia. The Equator passes through the center of this region and is influenced by seas and oceans from all sides.

nighttime (>20 °C) (Fig. 4b). In the projected years, the countries exhibit higher mean Ts (>40 °C) in the daytime, which is more noticeable in SSP5-8.5 and least noticeable in the SSP2-4.5 scenario (Fig. 4c). However, during nighttime, countries namely Armenia, Iran, Iraq, and Kyrgyzstan, predominantly exhibit the lowest Ts values in the SSP3-7.0 scenario (Fig. 4d).

The variation in the mean Ts during short-term (2026–2050), medium-term (2051–2075), and long-term (2076–2100) impacts under the four projected scenarios over the four geographic regions is shown in Fig. 5. In the short-term impact, the hot and dry region of the Arabian Peninsula (Region-1) shows lower mean Ts in SSP2-4.5 as compared to other three scenarios in daytime (Fig. 5a), while in nighttime a significant increase in mean Ts is evident from SSP1-2.6 to SSP5-8.5 (Fig. 5b). In contrast, there is a progressive increase in the mean Ts from SSP1-2.6 to SSP5-8.5 in both daytime and nighttime in medium- and long-term impacts. Considering the Indian Peninsula (Region-2), the mean Ts of SSP2-4.5 is lower than that of SSP1-2.6 for short-term impacts in both daytime and nighttime (Fig. 5c and d). The short-term impact in region-3 (Eastern China) exhibits a higher mean Ts in SSP3-7.0 in both daytime and nighttime (Fig. 5e). Region 4 of Indonesia and nearby countries witness a higher mean Ts in the SSP3-7.0 scenarios during the short-term impact. In contrast, the medium- and long-term impacts clearly show an increase in mean Ts, which is more significant in the high emission SSP5-8.5 scenario (Fig. 5g and h).

3.3. Hot spell days variation

The mean daytime hot spell days in the historical period were highest in region R4 (61 days), followed by regions R3, R2, and R1 (Table 4). Whereas, in the nighttime, region R2 witnessed more hot spell days (51

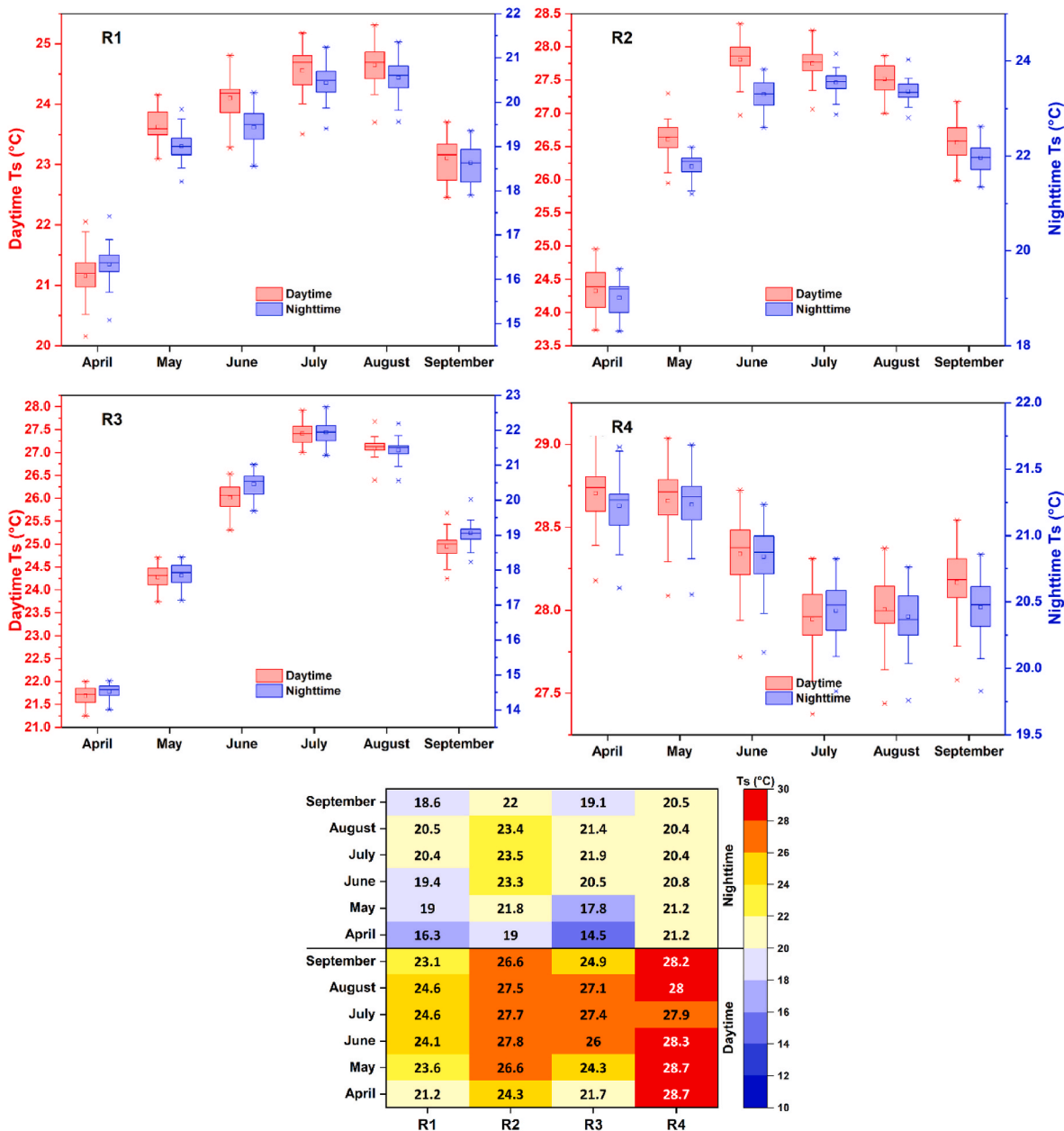


Fig. 3. Distribution of mean Ts of different summer months (April to September) over the four selected geographical regions (R1 to R4) in daytime and nighttime.

days) than regions R3, R4, and R1. This shows a strong daytime and nighttime control of hot spells across the selected geographic areas. Under the projected future scenarios, the R2 region shows significant growth in daytime hot spell days in the SSP5-8.5 scenario from 88 days in the short term to 115 days in the long term. A considerable increase in hot spell days in the long-term period of the SSP5-8.5 scenario is evident in region R4. In contrast, during nighttime, regions R2 and R3 will face higher hot spell days of 98 and 93 days, respectively, in long-term SSP5-8.5 scenarios.

3.4. Urban and rural population exposure to heat stress

The urban and rural population growth trajectories are different across different Asian countries, and thus, the examination of heat exposure to urban and rural populations separately is crucial for better future sustainability to heat vulnerability. The spatial map of daytime population exposure to heat stress in different urban and rural populations in four future scenarios of long-term (2076–2100) impact is

shown in Fig. 6. The historical period witnessed a higher heat stress population exposure along the Indo-Gangetic Plain of region R2 and the Eastern China region of R3 region. The long-term urban population exposure changes appeared significant in major parts of the Indo-Gangetic Plain in the SSP3-7.0 scenario (Fig. 6c). A considerably higher urban population exposure is observed along the Indo-Pak border area and in the southwestern Indian regions in the SSP3-7.0 and SSP5-8.5 scenarios, implying that more than 12 million people per year are exposed to heat stress conditions (Fig. 6c and d). The upsurge in population exposure is more rapid in the long-term than in the mid- and short-term impacts across all geographic regions, except region R3 (Eastern China), where a decline in population causes lower heat exposure in the long-term compared to the short-term period (Supplementary Figs. S3–S6). The population with higher income areas faces more heat stress as compared to the upper-middle income population (Supplementary Fig. S2).

The Arabian Peninsula region of R1 has significantly higher urban population exposure under long-term impacts in SSP3-7.0 (>0.9 million

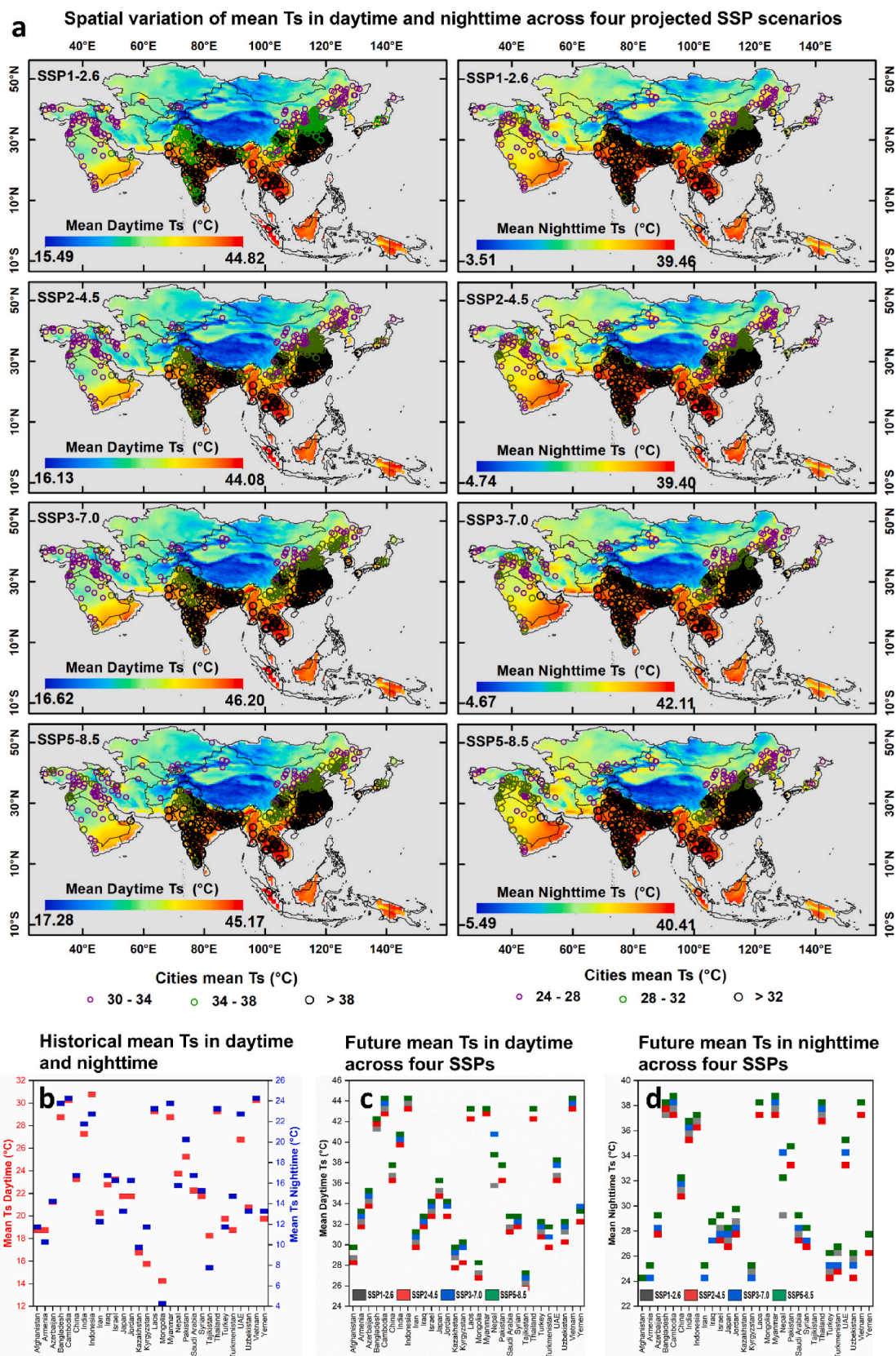


Fig. 4. (a) Projected change in mean Ts during daytime (left column) and nighttime (right column) over the selected regions under four different SSP scenarios, representing SSP1-2.6 (first row), SSP2-4.5 (second row), SSP3-7.0 (third row), and SSP5-8.5 (fourth row) during 2026–2100. The circle points represent the mean Ts over the selected cities with populations greater than 300k. Country-wise variation in mean Ts, (b) historical period in both daytime and nighttime, (c) four selected future SSP scenarios in the daytime, and (d) same as c for nighttime.

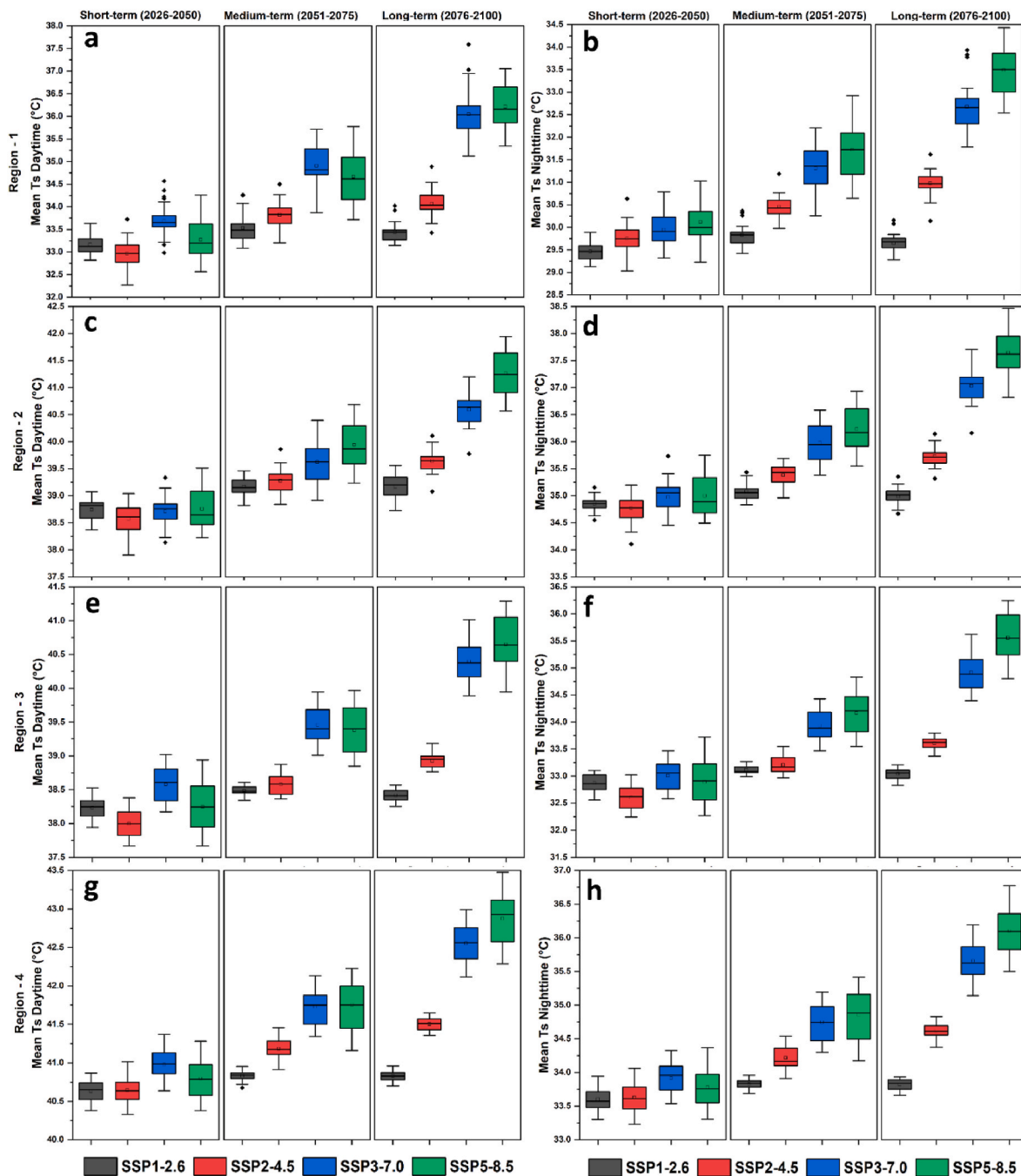


Fig. 5. Variation in mean Ts in projected years over the four selected geographic regions (as shown in Fig. 2a) under the SSP1-2.6, SSP2-4.5, SSP3-7.0, and SSP5-8.5 future scenarios during both daytime (a, c, e, and g in the left column) and nighttime (b, d, f, and h in the right column). Each scenario is further subdivided into three categories indicating short-term (2026–2050), medium-term (2051–2075), and long-term (2076–2100) impacts of each 25-year interval.

people per year), more in the daytime than at night (Fig. 7a). In contrast, rural population exposure behaves disproportionately, witnessing remarkably higher population exposure in SSP3-7.0 in the long term (~1.2 million people per year), while SSP2-4.5 had higher population exposure in the short term (Fig. 7b). Region R2, comprising one of the largest populous Indo-Gangetic Plains with high and upper-middle income populous, witnessed a massive urbanization rate in the SSP3 projection scenario. A gradual increase in urban population exposure to heat stress is evident over these regions from short-to long-term impacts in both daytime (Supplementary Fig. S3) and nighttime (Supplementary Fig. S4), with more significant increases in SSP3-7.0, accounting for more than 18 million people per year exposed to heat stress (Fig. 6a–d

and Fig. 7c), followed by SSP2-4.5 (~10 million people per year). Rural population exposure was much higher in SSP3-7.0 than in the other scenarios (Fig. 6g), with more than 9 million people per year exposed to heat stress (Fig. 7d) in the long-term impact. The heat stress population exposure in region R3 was extremely different from that in the other three geographic regions. There has been a substantial decline in urban population exposure seen in all the SSP scenarios (Fig. 7e) from short-term to long-term impacts in both daytime (Supplementary Fig. S5) and nighttime (Supplementary Fig. S6). A significant decline in daytime urban exposure is seen in SSP3-7.0 (from 4.5 to 4.1 million people per year) and SSP2-4.5 (from 4.9 to 3.9 million people per year) from short-term to long-term impacts. In contrast, rural population exposure was

Table 4
Number of hot spells in historical and four projected scenarios in three time periods during daytime and nighttime.

Region	Time-Period	Daytime				Nighttime					
		Historical	SSP1-2.6	SSP2-4.5	SSP3-7.0	SSP5-8.5	Historical	SSP1-2.6	SSP2-4.5	SSP3-7.0	SSP5-8.5
R1	Short-term	44	53	58	62	69	38	41	42	52	54
	Medium-term		63	66	65	74		51	51	59	65
	Long-term		68	70	79	82		53	59	70	73
R2	Short-term	54	66	61	71	88	51	56	61	64	69
	Medium-term		79	77	85	101		64	69	71	76
	Long-term		81	81	99	115		70	84	92	98
R3	Short-term	55	61	63	63	71	49	51	53	59	63
	Medium-term		64	68	76	86		60	61	65	74
	Long-term		72	76	90	99		67	74	88	92
R4	Short-term	61	68	69	80	89	48	49	52	60	65
	Medium-term		75	77	85	98		57	60	69	70
	Long-term		76	80	96	105		61	67	72	75

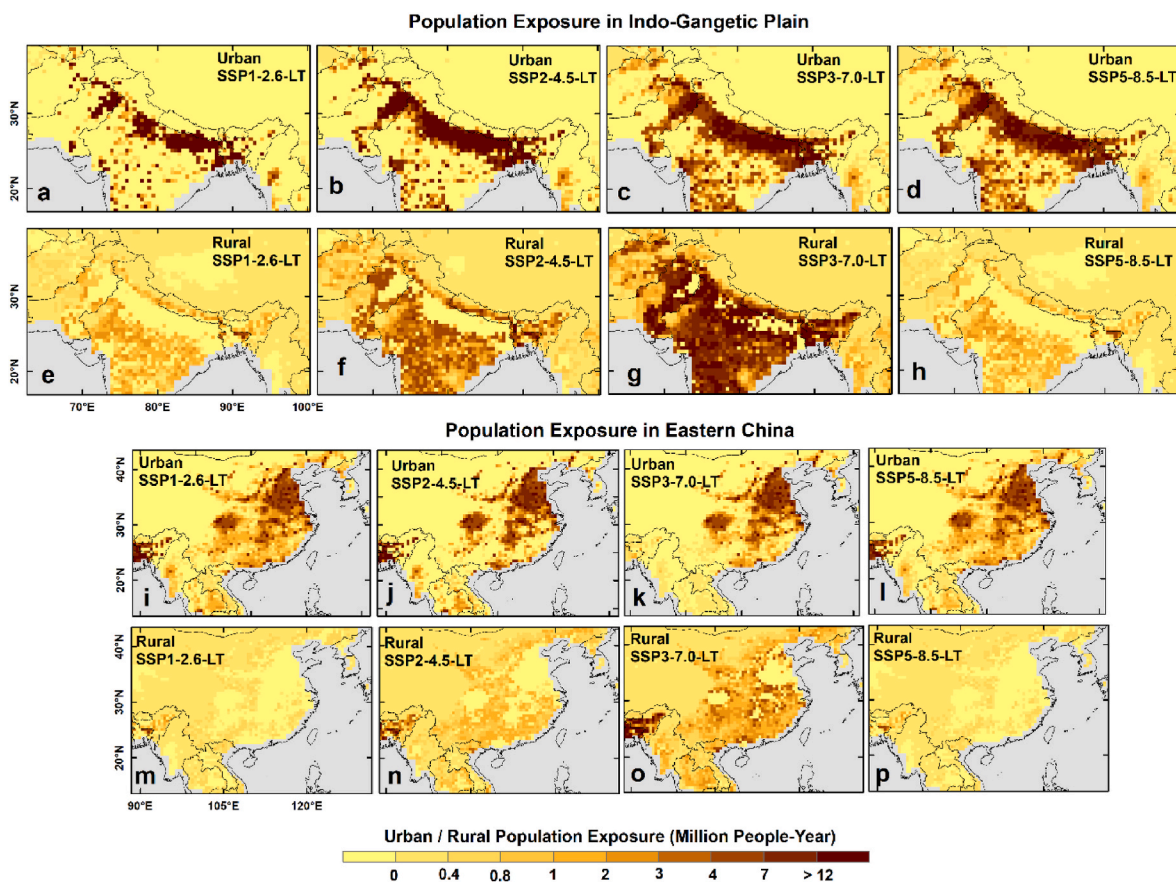


Fig. 6. Spatial distribution of mean daytime population exposure to heat stress in projected SSP1-2.6, SSP2-4.5, SSP3-7.0, and SSP5-8.5 scenarios of long-term (LT) impact (2076–2100) for urban and rural populations separately of the Indo-Gangetic Plain (a-d for urban and e-h for rural) and Eastern China (i-l for urban and m-p for rural) regions.

significantly higher in SSP3-7.0 (~1.5 million people per year) in the long-term impact (Figs. 7f and 6o). The population exposure of region R4 showed distinct variation at the day-to-day scale in both urban and rural contexts. There is increasing evidence of urban population exposure in SSP3-7.0 from short-term (1.3 million people per year) to long-term (1.8 million people per year) impacts in the daytime and from 1 to 1.5 million people per year in the nighttime (Fig. 5g).

4. Discussion

This study aims to assess heat stress variability in historical and future projected climate change and mitigation-based scenarios over four distinct geographic regions of Asia with varying climatic

conditions. The coastal region of the Arabian Peninsula shows a higher Ts due to the role of relative humidity from the surrounding seas and ocean in enhancing Ts (Al-Samarai, 2015), making them more susceptible to heat stress, especially in the daytime compared to nighttime. A previous study conducted in South Asia also observed higher historical heat stress along the Indo-Pak border region in both daytime and nighttime (Kyaw et al., 2023; Ullah 2022b). The Himalayan region’s complex topography and climatic conditions are responsible for making the Indo-Gangetic Plain region one of the most affected climate change-prone areas of the world (Norris et al., 2020). The human thermal discomfort conditions indicated higher anomalies along western India and the Indo-Gangetic region (Shukla & Attada, 2023). The role of irrigation (Krakauer et al., 2020; Mishra et al., 2020) and

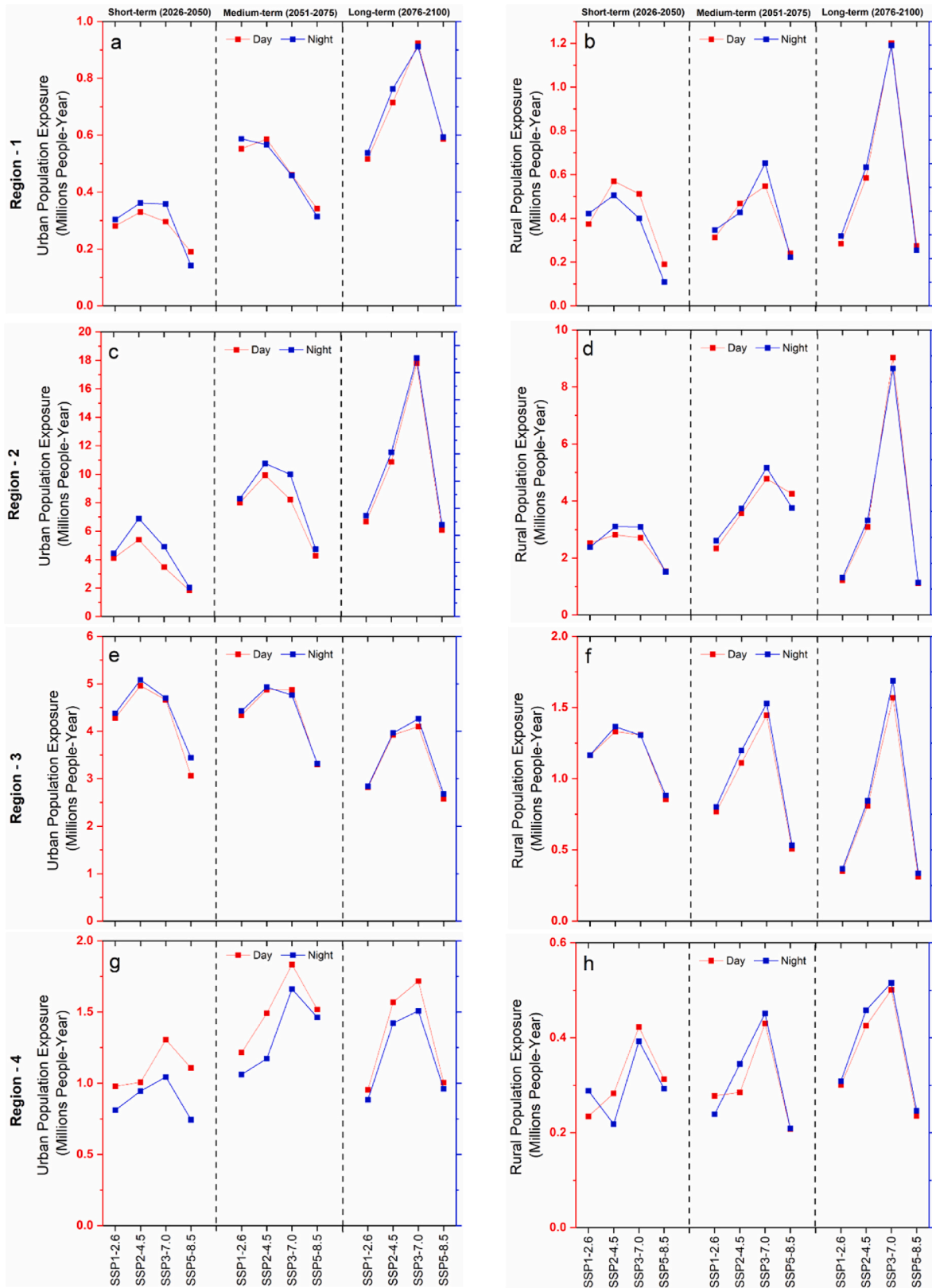


Fig. 7. Graphical representation of population exposure to heat stress per year under the SSP1-2.6, SSP2-4.5, SSP3-7.0, and SSP5-8.5 scenarios in short-term (2026–2050), medium-term (2051–2075), and long-term (2076–2100) impacts across the four geographic regions (R1 to R4) during both daytime and nighttime for urban (a, c, e, and g) and rural (b, d, f, and h) populations.

anthropogenic emissions is crucial in enhancing extreme heat stress phenomena (Allabakash & Lim, 2022; Han et al., 2020; Wang et al., 2021). Additionally, the atmospheric background plays a crucial role in generating heat waves in eastern China (Xie & Zhou, 2023). The study of heat waves and understanding their mechanics and dynamics is essential because they can cause a great loss to agriculture (Bai et al., 2021; Simpson et al., 2021) and reduce workability (Chakraborty et al., 2022). Thus, understanding the future heat stress situation will be crucial for preparedness and formulating mitigation strategies for future extreme heat stress conditions.

Most previous studies have focused on the projection of climate extremes at the global scale (Buzan & Huber, 2020; Mora et al., 2017; Qin, 2022; Sherwood & Huber, 2010); however, detailed studies on heat extremes over the Asian continent are limited. The outcomes of this study suggest that the mean T_s variation in projected years will be higher across a large part of Southern Asian countries with an upsurge in the daily T_s in all four SSP scenarios, with more significance in the SSP5-8.5 and SSP3-7.0 scenarios. Previously, using wet bulb temperature, it was estimated that the frequency of heat stress would increase by 70% in SSP2-4.5 and 90% in SSP5-8.5 in the western Indian region (Ullah 2022a). The present study's findings align with previous studies (Dimitrova et al., 2021; Rohini et al., 2019), which anticipated a significant increase in heat stress events in the projected RCP4.5 and RCP8.5 scenarios over South Asia. In summary, the T_s magnitude appears to have a relative persistence increase over South Asia with a high tendency from mid-latitudes to the tropics, which is also supported by previous studies (Buzan & Huber, 2020). The role of anticyclonic conditions (Ha et al., 2022) and large-scale atmospheric and oceanic circulation, particularly the El-Niño Southern Oscillation, plays a crucial role in the intensification of heat stress over the Asian region (Chowdary et al., 2014; Sein et al., 2021).

Heat-related mortality is supposed to increase in Asian cities under future climate change conditions (Zhou et al., 2022). Therefore, identifying the population exposed to heat stress conditions is necessary for a sustainable future. Previous studies mapped heat stress exposure based only on the total population (Freychet et al., 2022; Lohrey et al., 2021; Massaro et al., 2023; Qin, 2022; Sun et al., 2022; Ullah 2022a,b) and considered only two SSP scenarios, neglecting SSP3, in which a substantial increase in population will be observed (Jones & O'Neill, 2016). Since the vulnerability due to heat stress in urban and rural populations is different (López-Bueno et al., 2021), the present study aims to map the urban and rural population exposure to heat stress separately considering all four SSP scenarios, which is a main significant novel contribution of this research. The spatial and temporal population exposure of urban and rural regions in the four SSPs suggests a different trend across the four geographic regions in the three time periods. A significantly higher increase in urban population exposure is observed in South Asian countries (Im et al., 2017). In contrast, Eastern China shows a decrease in urban population exposure from the short to long term, which is mainly due to the declining population growth rate of China. Recent studies suggest a significant impact of higher population exposure on labour productivity (Lima, 2021), which indirectly affects the socio-economic status of a country. Thus, to minimize the effect of heat stress in future climatic conditions, it is advisable to control population growth, increase adaptive capacity, and increase the source of cooling infrastructure in buildings.

The present study focuses on the Asian region because of its dense population and higher vulnerability to heat stress. A more in-depth comprehensive understanding of the impact of urbanization level and heat intensification is recommended by examining a diverse range of urban settings, from megacities to smaller urban areas, and identifying global hotspots of heat stress. This study did not consider the mechanism of heat stress variability across different geographical regions, as such mechanisms have been previously explored, including the role of atmospheric control (insulation, precipitation, humidity, wind speed, etc.) (Xie & Zhou, 2023), aerosol and anthropogenic gas emission (Wang

et al., 2021), irrigation and moisture feedback (Mishra et al., 2020), and control of the El Niño Southern Oscillation (ENSO) and Indian Ocean Dipole (IOD) in modulating heat stress feedback (Mishra et al., 2022; Sein et al., 2021). Comparing different available heat stress indexes and their impact on future population exposure mapping could be another potential future research direction, as each heat index has its own strengths, limitations, and suitability across different geographical and climatic regions. Additionally, the inclusion of vulnerability mapping will be very helpful in identifying the regions of heat stress-vulnerable groups in future warming scenarios to which a population or region is susceptible to harm from heat stress, considering factors such as social, economic, and demographic characteristics.

5. Conclusion

The aim of the present research is to explore the diurnal variability of lethal heat stress over the four different geographic regions of Asia using the CMIP6 historical (1990–2014) and future climatic data (2026–2100) under four different SSP-RCP based future projected scenarios. The findings indicate that Southeast Asian countries, including Indonesia, the Philippines, Thailand, and Myanmar, experience higher mean thermal stress during the daytime due to their humid climate. In contrast, the Indo-Gangetic Plain and parts of the Indo-Pak border, characterized by a dry humid subtropical climate, show elevated mean historical T_s at night. Conversely, the dry, arid regions of the Arabian Peninsula exhibit lower mean T_s than the other three regions. The future projection of heat stress witnesses a significant increase in SSP5-8.5 and SSP3-7.0 climate projection scenarios in both daytime and nighttime. Additionally, this study examines population exposure mapping in different urban and rural areas across the SSPs scenarios. The Indo-Gangetic region marked a significantly higher population increase in the SSP3-7.0 scenario with long-term impact in both urban and rural areas. Although the amount of population exposure is higher in urban areas, the significantly higher growth in the SSP3-7.0 scenario is seen as compared to the other three scenarios in rural areas. In contrast, the urban population exposure in the eastern China region shows a decreasing trend from short-to long-term impact, while the rural population exposure shows an increasing trend that is more significant in the SSP3-7.0 scenario. The population exposure in the Arabian Peninsula and southeast Asian countries witnessed an increase in long-term impact, more in urban population than rural. The findings of this study underscore the urgent need for implementing effective mitigation measures to address extreme heat stress, ensuring a sustainable livelihood for populations in a warming climate.

CRedit authorship contribution statement

Pir Mohammad: Writing – original draft, Visualization, Software, Methodology, Investigation, Formal analysis, Data curation, Conceptualization. **Qihao Weng:** Writing – review & editing, Visualization, Validation, Supervision, Resources, Project administration, Methodology, Funding acquisition, Conceptualization.

Declaration of competing interest

The authors declare that there are no conflicts of interest relevant to this study.

Data availability statement

We are thankful to all the institutes and participating organizations for the development of Coupled Model Intercomparison Project Phase 6 (CMIP6) data products. The relative humidity and air temperature data is obtained from CMIP6 and detailed about the CMIP6 project can be found from <https://pcmdi.llnl.gov/CMIP6/>. The data for 26 different CMIP6 models is downloaded from the CMIP6 search interface,

available at <https://esgf-data.dkrz.de/search/cmip6-dkrz/> by searching for each individual model (the detailed list of each model can be found in [Supplementary Table 2](#)). Atmospheric reanalysis data are openly available for ERA5, which is used for biased correction of CMIP6 model data and can be easily downloaded from <https://cds.climate.copernicus.eu/cdsapp#!/dataset/reanalysis-era5-land-monthly-means?tab=form>. Gridded Population data is used to map the population exposure to heat stress for urban and rural region separately. Historical population data available at <https://www.isimip.org/gettingstarted/details/31/> and projected population data under different SSP scenarios obtained from the SEDAC website, available at <https://sedac.ciesin.columbia.edu/data/set/popdynamics-1-8th-pop-base-year-projection-ssp-2000-2100-rev01>. The open-source Python v3.9.13 has been used to process all the datasets using numeral packages including arcpy, Tkinter, tkinter, GDAL, etc. We have uploaded datasets containing the python scripts used to processing the time series data and the excel files used to generate the graphical figures in an online repository and can be available at <https://doi.org/10.5281/zenodo.10627775>.

Code availability

The Python code from this study is available from the corresponding author upon reasonable request.

Acknowledgments

We acknowledge the financial support of the Global STEM Professorship of Hong Kong SAR Government (P0039329), the Research Talent Hub of the Innovation and Technology Fund of Hong Kong (P0039329), Hong Kong Research Grants Council (15235524) and the Hong Kong Polytechnic University (P0046482 and P0038446) for this research.

Appendix A. Supplementary data

Supplementary data to this article can be found online at <https://doi.org/10.1016/j.habitatint.2025.103294>.

References

- Al-Samarai, M. (2015). Durability of Concrete in the Arabian Gulf. *Journal of Materials Science and Engineering*, 5(12), 398–408. <https://doi.org/10.17265/2161-6213/2015.11-12.003>
- Alizadeh, M. R., et al. (2022). Increasing heat-stress inequality in a warming climate. *Earth's Future*, 10(2), 1–11. <https://doi.org/10.1029/2021EF002488>
- Allabakash, S., & Lim, S. (2022). Anthropogenic influence of temperature changes across East Asia using CMIP6 simulations. *Scientific Reports*, 12(1), 1–14. <https://doi.org/10.1038/s41598-022-16110-9>
- Bai, H., et al. (2021). Multi-model ensemble of CMIP6 projections for future extreme climate stress on wheat in the North China plain. *International Journal of Climatology*, 41(S1), E171–E186. <https://doi.org/10.1002/joc.6674>
- Batibeniz, F., et al. (2020). Doubling of U.S. Population exposure to climate extremes by 2050. *Earth's Future*, 8(4), 1–14. <https://doi.org/10.1029/2019EF001421>
- Bi, D., et al. (2013). The ACCESS Coupled model: Description, control climate and preliminary Validation. *Australian Meteorological and Oceanographic Journal*, 63, 41–64.
- Boucher, O., et al. (2020). Presentation and evaluation of the IPSL-CM6A-LR climate model. *Journal of Advances in Modeling Earth Systems*, 12(7), 1–52. <https://doi.org/10.1029/2019MS002010>
- Buzan, J. R., & Huber, M. (2020). Moist heat stress on a hotter Earth. *Annual Review of Earth and Planetary Sciences*, 48, 623–655. <https://doi.org/10.1146/annurev-earth-053018-060100>
- Byun, Y.-H., et al. (2019). NIMS-KMA KACE1.0-G model output prepared for CMIP6 CMIP amp. Earth System Grid Federation. <https://doi.org/10.22033/ESGF/CMIP6.8350> [Preprint].
- Campbell-Lendrum, D., et al. (2023). Climate change and health: Three grand challenges. *Nature Medicine*, 29(7), 1631–1638. <https://doi.org/10.1038/s41591-023-02438-w>
- Cao, J., et al. (2018). The NUIST Earth system model (NESM) version 3: Description and preliminary evaluation. *Geoscientific Model Development*, 11(7), 2975–2993. <https://doi.org/10.5194/gmd-11-2975-2018>
- Chakraborty, T., et al. (2022). Lower urban humidity Moderates outdoor heat stress. *AGU Advances*, 3(5), 1–19. <https://doi.org/10.1029/2022AV000729>
- Chowdry, J. S., John, N., & Gnanaseelan, C. (2014). Interannual variability of surface air-temperature over India: Impact of ENSO and Indian Ocean Sea surface temperature. *International Journal of Climatology*, 34(2), 416–429. <https://doi.org/10.1002/joc.3695>
- Cvijanovic, I., et al. (2023). Importance of humidity for characterization and communication of dangerous heatwave conditions. *Npj Climate and Atmospheric Science*, 6(1), 15–17. <https://doi.org/10.1038/s41612-023-00346-x>
- Dimitrova, A., et al. (2021). Association between ambient temperature and heat waves with mortality in South Asia: Systematic review and meta-analysis. *Environment International*, 146. <https://doi.org/10.1016/j.envint.2020.106170>
- Dovie, D. B. K., & Pabi, O. (2023). Partial climatic risk screening, adaptation and livelihoods in a coastal urban area in Ghana. *Habitat International*, 138(October 2022), Article 102868. <https://doi.org/10.1016/j.habitatint.2023.102868>
- Dunne, J. P., et al. (2020). The GFDL Earth system model version 4.1 (GFDL-ESM 4.1): Overall Coupled model description and simulation characteristics. *Journal of Advances in Modeling Earth Systems*, 12(11), 1–56. <https://doi.org/10.1029/2019MS002015>
- Ec-Earth, E.-E. C. (2020). EC-Earth-Consortium EC-Earth3-Veg-LR model output prepared for CMIP6 CMIP historical. Earth System Grid Federation. <https://doi.org/10.22033/ESGF/CMIP6.4707>
- Ec-Earth, E.-E. C. (2021). EC-Earth-Consortium EC-Earth-3-CC model output prepared for CMIP6 CMIP historical. Earth System Grid Federation. <https://doi.org/10.22033/ESGF/CMIP6.4702>
- Eyring, V., et al. (2016). Overview of the Coupled model Intercomparison project Phase 6 (CMIP6) experimental design and organization. *Geoscientific Model Development*, 9(5), 1937–1958. <https://doi.org/10.5194/gmd-9-1937-2016>
- Fotso-Nguemo, T. C., et al. (2023). Projected impact of increased global warming on heat stress and exposed population over Africa. *Earth's Future*, 11(1), 1–17. <https://doi.org/10.1029/2022ef003268>
- Freychet, N., et al. (2022). Robust increase in population exposure to heat stress with increasing global warming. *Environmental Research Letters*, 17(6). <https://doi.org/10.1088/1748-9326/ac71b9>
- Fujibe, F. (2023). Climatology of heat stroke mortality in Japan. In *Climatological study of urban climate and heat and Cold Mortalities in Japan* (pp. 97–133). Singapore: Springer Nature Singapore. https://doi.org/10.1007/978-981-99-4386-9_5
- Garschagen, M. (2016). Decentralizing urban disaster risk management in a centralized system? Agendas, actors and contentions in Vietnam. *Habitat International*, 52, 43–49. <https://doi.org/10.1016/j.habitatint.2015.08.030>
- Gidden, M. J., et al. (2019). Global emissions pathways under different socioeconomic scenarios for use in CMIP6: A dataset of harmonized emissions trajectories through the end of the century. *Geoscientific Model Development*, 12(4), 1443–1475. <https://doi.org/10.5194/gmd-12-1443-2019>
- Goldewijk, K., et al. (2017). Anthropogenic land use estimates for the Holocene – HYDE 3.2. *Earth System Science Data*, 9(2), 927–953. <https://doi.org/10.5194/essd-9-927-2017>
- Gutjahr, O., et al. (2019). Max Planck institute Earth system model (MPI-ESM1.2) for the high-resolution model Intercomparison project (HighResMIP). *Geoscientific Model Development*, 12(7), 3241–3281. <https://doi.org/10.5194/gmd-12-3241-2019>
- Ha, K.-J., et al. (2022). Dynamics and characteristics of dry and moist heatwaves over East Asia. *Npj Climate and Atmospheric Science*, 5(1), 1–11. <https://doi.org/10.1038/s41612-022-00272-4>
- Hamed, K. H., & Ramachandra Rao, A. (1998). A modified Mann-Kendall trend test for autocorrelated data. *Journal of Hydrology*, 204(1–4), 182–196. [https://doi.org/10.1016/S0022-1694\(97\)00125-X](https://doi.org/10.1016/S0022-1694(97)00125-X)
- Han, W., et al. (2020). Opposite effects of aerosols on daytime urban heat island intensity between summer and Winter. *Atmospheric Chemistry and Physics*, (February), 1–36. <https://doi.org/10.5194/acp-2020-162>
- He, C., et al. (2021). Future global urban water scarcity and potential solutions. *Nature Communications*, 12(1), 1–11. <https://doi.org/10.1038/s41467-021-25026-3>
- Held, I. M., et al. (2019). Structure and performance of GFDL's CM4.0 climate model. *Journal of Advances in Modeling Earth Systems*, 11(11), 3691–3727. <https://doi.org/10.1029/2019MS001829>
- Hersbach, H., et al. (2020). The ERA5 global reanalysis. *Quarterly Journal of the Royal Meteorological Society*, 146(730), 1999–2049.
- Hussain, S. A., Nagaraja, S. B., & Menezes, R. G. (2016). Indian heat wave 2015: One of the deadliest in history. *Perspectives in Public Health*, 136(1), 6. <https://doi.org/10.1177/1757913915616725>
- Im, E.-S., Pal, J. S., & Eltahir, E. A. B. (2017). Deadly heat waves projected in the densely populated agricultural regions of South Asia. *Science Advances*, 3(e1603322), 1–7. <https://www.science.org>.
- Jiang, Y., Fu, P., & Weng, Q. (2015). Downscaling GOES land surface temperature for assessing heat wave health risks. *IEEE Geoscience and Remote Sensing Letters*, 12(8), 1605–1609. <https://doi.org/10.1109/LGRS.2015.2414897>
- Jones, B., & O'Neill, B. C. (2016). Spatially Explicit global population scenarios consistent with the shared socioeconomic pathways. *Environmental Research Letters*. <https://doi.org/10.1088/1748-9326/11/8/084003> [Preprint].
- Jones, B., & O'Neill, B. C. (2020). *Global one-Eighth Degree population base Year and projection grids based on the shared socioeconomic pathways, revision 01*. Palisades, New York: NASA Socioeconomic Data and Applications Center (SEDAC). <https://doi.org/10.7927/m30p-j498>
- Juckes, M., et al. (2020). The CMIP6 data request (DREQ, version 01.00.31). *Geoscientific Model Development*, 13(1), 201–224. <https://doi.org/10.5194/gmd-13-201-2020>
- Kendall, M. G. (1975). *Rank Correlation methods*. London: Charles Griffin ([Preprint]).
- Khan, N., et al. (2019). Trends in heat wave related indices in Pakistan. *Stochastic Environmental Research and Risk Assessment*, 33(1), 287–302. <https://doi.org/10.1007/s00477-018-1605-2>
- Kibwami, N., & Tutesigensi, A. (2016). Integrating clean development mechanism into the development approval process of buildings: A case of urban housing in Uganda.

- Habitat International, 53, 331–341. <https://doi.org/10.1016/j.habitatint.2015.12.011>
- Krakauer, N. Y., Cook, B. I., & Puma, M. J. (2020). Effect of irrigation on humid heat extremes. *Environmental Research Letters*, 15(9). <https://doi.org/10.1088/1748-9326/ab9ecf>
- Kyaw, A. K., Hamed, M. M., & Shahid, S. (2023). Spatiotemporal changes in Universal thermal climate index over South Asia. *Atmospheric Research*, 292(May). <https://doi.org/10.1016/j.atmosres.2023.106838>
- López-Bueno, J. A., et al. (2021). Analysis of the impact of heat waves on daily mortality in urban and rural areas in Madrid. *Environmental Research*, 195(February). <https://doi.org/10.1016/j.envres.2021.110892>
- Law, R. M., et al. (2017). The carbon cycle in the Australian Community climate and Earth system simulator (ACCESS-ESM1) - Part 1: Model description and pre-industrial simulation. *Geoscientific Model Development*, 10(7), 2567–2590. <https://doi.org/10.5194/gmd-10-2567-2017>
- Lee, W.-L., & Liang, H.-C. (2020). AS-RCEC TaiESM1.0 model output prepared for CMIP6 CMIP IptCO2. Earth System Grid Federation. <https://doi.org/10.22033/ESGF/CMIP6.9702> [Preprint].
- Li, D., et al. (2018). Extreme high-temperature events over East Asia in 1.5°C and 2°C warmer futures: Analysis of NCAR CESM low-warming Experiments. *Geophysical Research Letters*, 45(3), 1541–1550. <https://doi.org/10.1002/2017GL076753>
- Li, L., et al. (2020). The Flexible global ocean-Atmosphere-land system model grid-Point version 3 (FGOALS-g3): Description and evaluation. *Journal of Advances in Modeling Earth Systems*, 12(9), 1–28. <https://doi.org/10.1029/2019MS002012>
- Li, X., & Wang, S. (2022). Recent increase in the occurrence of Snow Droughts followed by extreme heatwaves in a warmer world. *Geophysical Research Letters* [Preprint]. <https://doi.org/10.1029/2022gl099925>
- Liu, Y., et al. (2020). Global socioeconomic risk of precipitation extremes under climate change. *Earth's Future*, 8(9), 1–15. <https://doi.org/10.1029/2019EF001331>
- Lima, C. Z., et al. (2021). Heat stress on agricultural workers exacerbates crop impacts of climate change. *Environmental Research Letters*, 16(4). <https://doi.org/10.1088/1748-9326/abeb9f>
- Liu, M., et al. (2021). Non-stationary frequency analysis of extreme streamflow disturbance in a typical ecological function reserve of China under a changing climate. *Ecohydrology*, 14(7), 1–20. <https://doi.org/10.1002/eco.2323>
- Lohrey, S., et al. (2021). Deadly heat exposure in an urbanized world. *EarthArXiv* [Preprint], (January 2023). <https://eartharxiv.org/repository/view/2754/>
- Lovato, T., et al. (2022). CMIP6 simulations with the CMCC Earth system model (CMCC-ESM2). *Journal of Advances in Modeling Earth Systems*, 14(3). <https://doi.org/10.1029/2021MS002814>
- Malik, S., et al. (2020). Trend of extreme rainfall events using suitable Global Circulation Model to combat the water logging condition in Kolkata Metropolitan Area. *Urban Climate*, 32, Article 100599. <https://doi.org/10.1016/j.uclim.2020.100599>
- Mann, H. B. (1945). Nonparametric tests against trend. *Econometrica*, 13(3), 245–259. <https://doi.org/10.1016/j.econometrica.2004.07.001>
- Massaro, E., et al. (2023). Spatially-optimized urban greening for reduction of population exposure to land surface temperature extremes. *Nature Communications*, 14(1), 2903. <https://doi.org/10.1038/s41467-023-38596-1>
- Massonnet, F., et al. (2020). Replicability of the EC-Earth3 Earth system model under a change in computing environment. *Geoscientific Model Development*, 13(3), 1165–1178. <https://doi.org/10.5194/gmd-13-1165-2020>
- Mauritsen, T., et al. (2019). Developments in the MPI-M Earth system model version 1.2 (MPI-ESM1.2) and its response to increasing CO2. *Journal of Advances in Modeling Earth Systems*, 11(4), 998–1038. <https://doi.org/10.1029/2018MS001400>
- Meehl, G. A., & Tebaldi, C. (2004). More intense, more frequent, and longer lasting heat waves in the 21st century. *Science*, 305(5686), 994–997. <https://doi.org/10.1126/science.1098704>
- Mishra, V., et al. (2020). Moist heat stress extremes in India enhanced by irrigation. *Nature Geoscience*, 13(11), 722–728. <https://doi.org/10.1038/s41561-020-00650-8>
- Mishra, V., Tiwari, A. D., & Kumar, R. (2022). Warming climate and ENSO variability enhance the risk of sequential extremes in India. *One Earth*, 5(11), 1250–1259. <https://doi.org/10.1016/j.oneear.2022.10.013>
- Mohammad, P., & Goswami, A. (2021). Quantifying diurnal and seasonal variation of surface urban heat island intensity and its associated determinants across different climatic zones over Indian cities. *GIScience and Remote Sensing*, 58(7), 955–981. <https://doi.org/10.1080/15481603.2021.1940739>
- Mohammad, P., & Weng, Q. (2024). Comparing existing heat wave indices in identifying dangerous heat wave outdoor conditions. *Nexus*, 1(3), Article 100027. <https://doi.org/10.1016/j.nexus.2024.100027>
- Mora, C., et al. (2017). Global risk of deadly heat. *Nature Climate Change*, 7(7), 501–506. <https://doi.org/10.1038/nclimate3322>
- Nanditha, J. S., et al. (2020). A seven-fold rise in the probability of exceeding the observed hottest summer in India in a 2°C warmer world. *Environmental Research Letters*, 15(4). <https://doi.org/10.1088/1748-9326/ab7555>
- Norris, J., et al. (2020). Warming and drying over the central Himalaya caused by an amplification of local mountain circulation. *Npj Climate and Atmospheric Science*, 3(1), 1–11. <https://doi.org/10.1038/s41612-019-0105-5>
- O'Neill, B. C., et al. (2016). The scenario model Intercomparison project (ScenarioMIP) for CMIP6. *Geoscientific Model Development*, 9(9), 3461–3482. <https://doi.org/10.5194/gmd-9-3461-2016>
- Pal, J. S., & Eltahir, E. A. B. (2016). Future temperature in southwest Asia projected to exceed a threshold for human adaptability. *Nature Climate Change*, 6(2), 197–200. <https://doi.org/10.1038/nclimate2833>
- Qin, P. (2022). More than six billion people encountering more exposure to extremes with 1.5 °C and 2.0 °C warming. *Atmospheric Research*, 273(March), Article 106165. <https://doi.org/10.1016/j.atmosres.2022.106165>
- Rohini, P., Rajeevan, M., & Mukhopadhyay, P. (2019). Future projections of heat waves over India from CMIP5 models. *Climate Dynamics*, 53(1), 975–988. <https://doi.org/10.1007/s00382-019-04700-9>
- Ruosteenoja, K., et al. (2017). Surface air relative humidities spuriously exceeding 100% in CMIP5 model output and their impact on future projections. *Journal of Geophysical Research: Atmospheres*, 122(18), 9557–9568. <https://doi.org/10.1002/2017JD026909>
- Saeed, F., Schlessner, C. F., & Ashfaq, M. (2021). Deadly heat stress to become commonplace across South Asia already at 1.5°C of global warming. *Geophysical Research Letters*, 48(7), 1–11. <https://doi.org/10.1029/2020GL091191>
- Sein, Z. M. M., et al. (2021). Interannual variability of air temperature over Myanmar: The influence of ENSO and IOD. *Climate*, 9(2), 1–19. <https://doi.org/10.3390/cli9020035>
- Seland, Ø., et al. (2020). Overview of the Norwegian Earth System Model (NorESM2) and key climate response of CMIP6 DECK, historical, and scenario simulations. *Geoscientific Model Development*. <https://doi.org/10.5194/gmd-13-6165-2020>
- Semmler, T., et al. (2020). Simulations for CMIP6 with the AWI climate model AWI-CM-1-1. *Journal of Advances in Modeling Earth Systems*, 12(9), 1–34. <https://doi.org/10.1029/2019MS002009>
- Sen, K. P. (1968). Estimates of the regression Coefficient based on Kendall's Tau Pranab Kumar sen. *Journal of the American Statistical Association*, 63(324), 1379–1389. <https://doi.org/10.1080/01621459.1968.10480934>
- Sherwood, S. C., & Huber, M. (2010). An adaptability limit to climate change due to heat stress. *Proceedings of the National Academy of Sciences of the United States of America*, 107(21), 9552–9555. <https://doi.org/10.1073/pnas.0913352107>
- Shukla, K. K., & Attada, R. (2023). CMIP6 models informed summer human thermal discomfort conditions in Indian regional hotspot. *Scientific Reports*, 13(1), Article 12549. <https://doi.org/10.1038/s41598-023-38602-y>
- Simpson, C., et al. (2021). Regional disparities and seasonal differences in climate risk to rice labour. *Environmental Research Letters*, 16(12). <https://doi.org/10.1088/1748-9326/ac3288>
- Stull, R. (2011). Wet-bulb temperature from relative humidity and air temperature. *Journal of Applied Meteorology and Climatology*, 50(11), 2267–2269. <https://doi.org/10.1175/JAMC-D-11-0143.1>
- Sun, X., et al. (2022). Will population exposure to heat extremes intensify over Southeast Asia in a warmer world? *Environmental Research Letters*, 17(4). <https://doi.org/10.1088/1748-9326/ac48b6>
- Swart, N. C., et al. (2019). The Canadian Earth system model version 5 (CanESM5.0.3). *Geoscientific Model Development*, 12(11), 4823–4873. <https://doi.org/10.5194/gmd-12-4823-2019>
- Tatebe, H., et al. (2019). Description and basic evaluation of simulated mean state, internal variability, and climate sensitivity in MIROC6. *Geoscientific Model Development*, 12(7), 2727–2765. <https://doi.org/10.5194/gmd-12-2727-2019>
- Tuholske, C., et al. (2021). Global urban population exposure to extreme heat. *PNAS*, 118(41), 1–9. <https://doi.org/10.1073/pnas.2024792118>
- Ullah, I., et al. (2022a). Projected changes in socioeconomic exposure to heatwaves in South Asia under changing climate. *Earth's Future*, 10(2), 1–19. <https://doi.org/10.1029/2021EF002240>
- Ullah, S., et al. (2022b). Future population exposure to daytime and nighttime heat waves in South Asia. *Earth's Future*, 10(5), 1–16. <https://doi.org/10.1029/2021EF002511>
- Van Noije, T., et al. (2021). EC-Earth3-AerChem: A global climate model with interactive aerosols and atmospheric chemistry participating in CMIP6. *Geoscientific Model Development*, 14(9), 5637–5668. <https://doi.org/10.5194/gmd-14-5637-2021>
- Volodin, E. M., et al. (2017). Simulation of the present-day climate with the climate model INMCM5. *Climate Dynamics*, 49(11), 3715–3734. <https://doi.org/10.1007/s00382-017-3539-7>
- Volodin, E. M., et al. (2018). Simulation of the modern climate using the INM-CM48 climate model. *Russian Journal of Numerical Analysis and Mathematical Modelling*, 33(6), 367–374.
- Vuuren, D. P., et al. (2011). The representative concentration pathways: An overview. *Climatic Change*, 109(1), 5–31. <https://doi.org/10.1007/s10584-011-0148-z>
- Wallemacq, P., & House, R. (2018). Economic losses, poverty and disasters 1998–2017, united Nations Office for disaster risk reduction. <https://www.undrr.org/publication/economic-losses-poverty-disasters-1998-2017>
- Wang, S. S. Y., et al. (2019). Consecutive extreme flooding and heat wave in Japan: Are they becoming a norm? *Atmospheric Science Letters*, 20(10), 2–5. <https://doi.org/10.1002/asl.933>
- Wang, J., et al. (2021). Anthropogenic emissions and urbanization increase risk of compound hot extremes in cities. *Nature Climate Change*, 11(12), 1084–1089. <https://doi.org/10.1038/s41558-021-01196-2>
- Wouters, H., et al. (2022). Soil drought can mitigate deadly heat stress thanks to a reduction of air humidity. *Science Advances*, 8(1), 1–12. <https://doi.org/10.1126/sciadv.abe6653>
- Wu, T., et al. (2019). The Beijing Climate center climate system model (BCC-CSM): The main progress from CMIP5 to CMIP6. *Geoscientific Model Development*, 12(4), 1573–1600. <https://doi.org/10.5194/gmd-12-1573-2019>
- Wyser, K., et al. (2020). On the increased climate sensitivity in the EC-Earth model from CMIP5 to CMIP6. *Geoscientific Model Development*, 13(8), 3465–3474. <https://doi.org/10.5194/gmd-13-3465-2020>
- Xie, W., & Zhou, B. (2023). On the atmospheric background for the occurrence of three heat wave types in East China. *Weather and Climate Extremes*, 39(August 2022), Article 100539. <https://doi.org/10.1016/j.wace.2022.100539>
- Xu, Z., et al. (2021). Bias-corrected CMIP6 global dataset for dynamical downscaling of the historical and future climate (1979–2100). *Scientific Data*, 8(1), 1–11. <https://doi.org/10.1038/s41597-021-01079-3>

- Yin, C., et al. (2022). Changes in global heat waves and its socioeconomic exposure in a warmer future. *Climate Risk Management*, 38, Article 100459. <https://doi.org/10.1016/j.crm.2022.100459>
- Yukimoto, S., et al. (2019). The meteorological research institute Earth system model version 2.0, MRI-ESM2.0: Description and basic evaluation of the physical Component. *Journal of the Meteorological Society of Japan. Ser. II*, 97(5), 931–965. <https://doi.org/10.2151/jmsj.2019-051>
- Zhai, J., et al. (2020). Future drought characteristics through a multi-model ensemble from CMIP6 over South Asia. *Atmospheric Research*, 246(April), Article 105111. <https://doi.org/10.1016/j.atmosres.2020.105111>
- Zhou, L., et al. (2022). The burden of heat-related stroke mortality under climate change scenarios in 22 East Asian cities. *Environment International*, 170(September), Article 107602. <https://doi.org/10.1016/j.envint.2022.107602>